JOURNAL OF THE CHINESE CHEMICAL SOCIETY

Mini Review

Theory and Applications of Sum-Frequency Generations

C. K. Lin,[a,b] L. Yang,[a,c,*] M. Hayashi,[d,*] C. Y. Zhu,[a] Y. Fujimura,[a,b] Y. R. Shen[e] and S. H. Lin[a,b,*]

[a]*Department of Applied Chemistry, Institute of Molecular Science and Center for Interdisciplinary Molecular Science, National Chiao-Tung University, Hsinchu 30050, Taiwan*

[b]*Institute of Atomic and Molecular Sciences, Academia Sinica, Taipei, Taiwan*

[c]*Institute of Theoretical and Simulation Chemistry, Academy of Fundamental and Interdisciplinary Science, Harbin Institute of Technology, Harbin 150080, PR China*

[d]*Center for Condensed Matter Sciences, National Taiwan University, Taipei, Taiwan*

[e]*Department of Physics, University of California, Berkeley, California, USA*

(Received: Aug. 9, 2013; Accepted: Aug. 13, 2013; Published Online: Oct. 7, 2013; DOI: 10.1002/jccs.201300416)

The SFG technique has become popular since the pioneering work conducted by Shen's group in late 1980s. Combined the advantages of other surface-detecting techniques, the SFG technique could identify both chemical species and orientations adsorbed on surfaces or inserted between surfaces. In view of the recent tremendous experimental activities of SFG in surface chemistry, biochemistry and material sciences, quantum chemical calculations of SFG spectra to analyze the experimental SFG spectra are badly needed. In this paper we presented the theoretical expressions of various SFG techniques and showed how to employ the quantum chemical calculations to simulate the corresponding SFG spectra.

Keywords: Spectroscopy; Nonlinear optical processes; Susceptibility method.

Prof. S. H. Lin *is currently a professor at the Department of Applied Chemistry, National Chiao Tung University. He is also an academician of the Academia Sinica, Taiwan. Prof. Lin received his Bachelor's Degree in 1958 and Master's Degree in 1960 in Chemistry from National Taiwan University. He obtained Ph.D. from University of Utah in 1964. He was an Assistant Professor (1965-1968), Associate Professor (1968-1972), and was promoted to professorship 1972~1995 in Department of Chemistry, Arizona State University. He was the Director of Institute of Atomic and Molecular Sciences, Academia Sinica (1993-2007). He has contributed research efforts in the fields of physical chemistry, photochemistry, and theoretical chemistry. He has received several awards including Alexander von Humboldt Foundation, U.S. Senior Scientist Award (1979-1980, 1986, 1993), Kai-Ying Tsing Distinguished Lecturer (1993), Eminent Scientist of RIKEN (1995), and Taiwanese American Foundation Prize (1995).*

Special Issue for the 60th Anniversary of Journal of the Chinese Chemical Society

* Corresponding author. Tel: +886-3-5712121#56591; Fax: +886-3-5723764;
Email: sheng@mail.nctu.edu.tw, atmyh@ntu.edu.tw, yangling@hit.edu.cn

INTRODUCTION

The SFG technique has become available on analyzing surface species since the works conducted by Shen's group in late 1987.[1,2] With an optical parametric amplifier tuned around 2800 to 3100 cm^{-1} with a frequency-doubled Nd:YAG laser, they have successfully recorded IR-Vis SFG spectra of methanol and pentadecanoic acid (PDA) adsorbed on glass and on water surface. By tuning the IR frequency, different vibrational resonances were obtained, and with various combinations of incident beam polarizations (s and/or p), different C-H stretching modes were revealed. They have further analyzed C-H vibration signals of PDA at different adsorption densities, finding the long alkane chains nearly oriented straightly along the normal to the water surface in the liquid-condensed phase at high density.[2]

Following these pioneering works, numerous applications of vibrational SFG spectroscopy to surface chemistry, biochemistry and material sciences emerged. One major category of experiments focused on the orientations of functional groups of organic polymers adsorbed on solid surfaces.[3-9] Aliphatic and aromatic C-H stretching modes from different chemical species could be distinguished by resonance frequencies, and their orientations could be deduced from signal intensities recorded under different combinations of incident/output beam polarizations. The results showed some substrate-dependence of the adsorbate orientation. For example, the phenyl groups in polystyrene have an average tilt angle of ~20° at the polystyrene-air interface when the polymer is adsorbed on sapphire, and ~57° on oxidized silicon substrate.[5,6] It should be noted that there exist several types of vibrational SFG and electronic SFG. In addition to VSFG, Tahara and coworkers have recently made heterodyne-detected electronic sum-frequency generation (ESFG) applicable.[10-12] In their experiments, two visible/near-infrared beams were guided to the sample where the sum frequency was tuned resonant with an electronic state. By this means the orientation distribution of surfactant-like molecules floating on water surface could be resolved and, furthermore, the pH value of water surface was claimed.[13-15] It should be noticed that, however, a solid theoretical framework to interpret these important experimental results is still in demand. The SFG technique could identify both chemical species and orientations at the same time, which combines the advantages of other surface-detecting techniques such as Raman scattering, atomic force microscopy, and X-ray spectroscopy.

In view of the above-mentioned rapid developments of SFG spectroscopies, in this paper we shall present the theoretical expressions of various SFG techniques and show how to employ the quantum chemical calculations to analyze and simulate the corresponding SFG spectra. We shall also give a brief review of SFG experiments in chemistry, biology and surface science.

THEORY — SUSCEPTIBILITY METHOD

To treat nonlinear optical processes, the susceptibility method is commonly used. The central problem in the susceptibility method is to calculate the polarization $\vec{P}$ which is an ensemble average of dipole moment $\vec{\mu}$, i.e.

$$\vec{P} = Tr(\hat{\rho}\vec{\mu}) = Tr(\vec{\mu}\hat{\rho}) \tag{2-1}$$

where $\hat{\rho}$ denotes the density matrix of the system. The diagonal and off-diagonal elements of $\hat{\rho}$ describe the population and phase (or coherence) of the system, respectively. Notice that the equation of motion for the density matrix $\hat{\rho}(t)$ of the system is given by the stochastic Liouville equation[16]

$$\begin{aligned}\frac{\partial\hat{\rho}}{\partial t} &= -i\hat{L}_0\hat{\rho} - \hat{\Gamma}\hat{\rho} - i\hat{L}'(t)\hat{\rho} = -\frac{i}{\hbar}\left[\hat{H}_0,\hat{\rho}\right] - \hat{\Gamma}\hat{\rho} - \frac{i}{\hbar}\left[\hat{V}(t),\hat{\rho}\right] \\ &= -i\hat{L}_0\hat{\rho} - \frac{i}{\hbar}\left[\hat{V},\hat{\rho}\right]\end{aligned} \tag{2-2}$$

where $i\hat{L}_0' = i\hat{L}_0 + \hat{\Gamma}$, and $\hat{L}_0$ and $\hat{L}'(t)$ denote the Liouville operators corresponding to the zeroth-order Hamiltonian and Hamiltonian for the interaction $\hat{V}$ between the system and radiation field, respectively. $\hat{\Gamma}$ denotes the damping operator describing the relaxation and dephasing of the system. To evaluate $\vec{P}$, it is necessary to solve Eq. (2-2). For this purpose, for the weak field case the perturbation method is often used. This can be carried out by regarding $\hat{L}'$ in Eq. (2-2) as a perturbation and solving Eq. (2-2) directly.

For SFG, we have to evaluate the second-order polarization $\hat{P}^{(2)}(t)$ given by [17]

$$\vec{P}^{(2)}(t) = Tr\left(\hat{\rho}^{(2)}\vec{\mu}\right) \tag{2-3}$$

In the dipole approximation, one can write $\hat{V}(t)$ as

$$\hat{V}(t) = -\sum_{i}^{2}\sum_{\alpha_i}\vec{\mu}\cdot\vec{E}(\alpha_i\omega_i)e^{-it\alpha_i\omega_i}l_i(t) \tag{2-4}$$

and

$$l_i(t) = e^{-(t_p - t)/T_i} \tag{2-5}$$

where $\vec{\mu}$ represents the dipole operator, α_i takes the value 1 or –1 and $l_i(t)$ denotes the laser pulse-shape function with pulse duration T_i. The summation over i in Eq. (2-4) describes the situation that in SFG two lasers are involved.

Equation (2-3) is general and can be applied to study difference-frequency and sum-frequency generations. For SFG, for convenience, Eq. (2-3) can be written as

$$\begin{aligned}\vec{P}^{(2)}(t_p) = {} & \vec{P}^{(2)}(\omega_1+\omega_2)\exp\left[-it_p(\omega_1+\omega_2)\right] \\ & + \vec{P}^{(2)}(-\omega_1-\omega_2)\exp\left[it_p(\omega_1+\omega_2)\right]\end{aligned} \tag{2-6}$$

where

$$\begin{aligned}\vec{P}^{(2)}(\omega_1+\omega_2) = {} & \frac{(-i)^2}{(\hbar)^2}\sum_k\sum_{k'}\sum_l\left\{\frac{\vec{\mu}_{lk}\Delta\sigma(lk)}{\left[i(\omega'_{kl}-\omega_i-\omega_j)+1/T_1+1/T_2\right]}\sum_i\sum_{j}^{i\neq j}\frac{\left[\vec{\mu}_{kl}\cdot\vec{E}_i(\omega_i)\right]\left[\vec{\mu}_{kk}\cdot\vec{E}_j(\omega_j)\right]}{\left[i(\omega'_{kl}-\omega_i)+1/T_i\right]}\right. \\ & + \frac{\vec{\mu}_{lk}\Delta\sigma(kk)}{\left[i(\omega'_{kl}-\omega_i-\omega_j)+1/T_1+1/T_2\right]}\sum_i\sum_{j}^{i\neq j}\frac{\left[\vec{\mu}_{kk}\cdot\vec{E}_i(\omega_i)\right]\left[\vec{\mu}_{kl}\cdot\vec{E}_j(\omega_j)\right]}{\left[i(\omega'_{kk}-\omega_i)+1/T_i\right]} \\ & + \left[\frac{\vec{\mu}_{lk}\Delta\sigma(lk)}{\left[i(\omega'_{kl}+\omega_i+\omega_j)+1/T_1+1/T_2\right]}\sum_i\sum_{j}^{i\neq j}\frac{\left[\vec{\mu}_{kl}\cdot\vec{E}_i(-\omega_i)\right]\left[\vec{\mu}_{kk}\cdot\vec{E}_j(-\omega_j)\right]}{\left[i(\omega'_{kl}+\omega_i)+1/T_i\right]}\right. \\ & \left.\left. + \frac{\vec{\mu}_{lk}\Delta\sigma(kk)}{\left[i(\omega'_{kl}+\omega_i+\omega_j)+1/T_1+1/T_2\right]}\sum_i\sum_{j}^{i\neq j}\frac{\left[\vec{\mu}_{kk}\cdot\vec{E}_i(-\omega_i)\right]\left[\vec{\mu}_{kl}\cdot\vec{E}_j(-\omega_j)\right]}{\left[i(\omega'_{kk}+\omega_i)+1/T_i\right]}\right]^*\right\}\end{aligned} \tag{2-7}$$

and, for example, $\hat{\sigma}_i = e^{i\hat{L}_0 t_i}\hat{\rho}_i$, $\Delta\sigma(lk') \equiv (\hat{\sigma}_i)_{ll} - (\hat{\sigma}_i)_{k'k'}$ representing the initial distributions of the system. In other words, in SFG the coefficient of $\exp[-it_p(\omega_1+\omega_2)]$ or $\exp[it_p(\omega_1+\omega_2)]$ should be needed. Here in the double summations over i and j, the $i = j$ terms are to be excluded.

One can consider an energy level diagram for SFG as shown in Fig. 1. In Fig. 1, g, m and k denote the initial, intermediate and final state manifolds, and ω_1 and ω_2 represent the frequencies of the two lasers used in SFG experiments.

According to the definition of the second-order non-

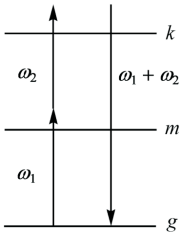

Fig. 1. Energy level diagram for off-resonance–off-resonance SFG.

linear susceptibility $\chi^{(2)}_{\alpha\beta\gamma}(\omega_1+\omega_2)$ for SFG,

$$\vec{P}^{(2)}_{\alpha}(\omega_1+\omega_2) = \sum_{\beta}\sum_{\gamma}\chi^{(2)}_{\alpha\beta\gamma}(\omega_1+\omega_2)E_{1\beta}(\omega_1)E_{2\gamma}(\omega_2) \tag{2-8}$$

where α, β and γ denote the space-fixed coordinates X, Y and/or Z, it is found

$$\chi^{(2)}_{\alpha\beta\gamma}(\omega_1+\omega_2) = \chi^{(2)}_{\alpha\beta\gamma}(\omega_1+\omega_2)_1 + \chi^{(2)}_{\alpha\beta\gamma}(\omega_1+\omega_2)_2 + \chi^{(2)}_{\alpha\beta\gamma}(\omega_1+\omega_2)_3 \tag{2-9}$$

where

$$\begin{aligned}\chi^{(2)}_{\alpha\beta\gamma}(\omega_1+\omega_2)_1 = {} & \frac{i^2}{\hbar^2}\sum_g\sum_k\sum_m\Delta\sigma(gm) \\ & \times\left\{\mu_{gk}(\alpha)\left[\frac{\mu_{mg}(\beta)\mu_{km}(\gamma)}{\left[i(\omega_{mg}-\omega_1)+\Gamma'_{mg}\right]\left[i(\omega_{kg}-\omega_1-\omega_2)+\Gamma'_{kg}\right]}\right.\right. \\ & \left. + \frac{\mu_{mg}(\gamma)\mu_{km}(\beta)}{\left[i(\omega_{mg}-\omega_2)+\Gamma''_{mg}\right]\left[i(\omega_{kg}-\omega_1-\omega_2)+\Gamma'_{kg}\right]}\right] \\ & + \mu_{kg}(\alpha)\left[\frac{\mu_{mg}(\beta)\mu_{km}(\gamma)}{\left[i(\omega_{mg}+\omega_1)+\Gamma'_{mg}\right]\left[i(\omega_{kg}+\omega_1+\omega_2)+\Gamma'_{kg}\right]}\right. \\ & \left.\left. + \frac{\mu_{mg}(\gamma)\mu_{km}(\beta)}{\left[i(\omega_{mg}+\omega_2)+\Gamma''_{mg}\right]\left[i(\omega_{kg}+\omega_1+\omega_2)+\Gamma'_{kg}\right]}\right]^* \\ & - \mu_{mk}(\alpha)\left[\frac{\mu_{gm}(\beta)\mu_{kg}(\gamma)}{\left[i(\omega_{gm}-\omega_1)+\Gamma'_{mg}\right]\left[i(\omega_{km}-\omega_1-\omega_2)+\Gamma'_{km}\right]}\right. \\ & \left. + \frac{\mu_{gm}(\gamma)\mu_{kg}(\beta)}{\left[i(\omega_{gm}-\omega_2)+\Gamma''_{mg}\right]\left[i(\omega_{km}-\omega_1-\omega_2)+\Gamma'_{km}\right]}\right] \\ & - \mu_{km}(\alpha)\left[\frac{\mu_{gm}(\beta)\mu_{kg}(\gamma)}{\left[i(\omega_{gm}+\omega_1)+\Gamma'_{mg}\right]\left[i(\omega_{km}+\omega_1+\omega_2)+\Gamma'_{km}\right]}\right. \\ & \left.\left. + \frac{\mu_{gm}(\gamma)\mu_{kg}(\beta)}{\left[i(\omega_{gm}+\omega_2)+\Gamma''_{mg}\right]\left[i(\omega_{km}+\omega_1+\omega_2)+\Gamma'_{km}\right]}\right]^*\right\}\end{aligned} \tag{2-10}$$

$\chi^{(2)}_{\alpha\beta\gamma}(\omega_1+\omega_2)_2$ and $\chi^{(2)}_{\alpha\beta\gamma}(\omega_1+\omega_2)_3$ can be obtained from $\chi^{(2)}_{\alpha\beta\gamma}(\omega_1+\omega_2)_1$ by performing the exchanges $k \leftrightarrow m$ and $k \leftrightarrow g$, respectively. The expressions for $\chi^{(2)}_{\alpha\beta\gamma}(\omega_1+\omega_2)_2$ and $\chi^{(2)}_{\alpha\beta\gamma}(\omega_1+\omega_2)_3$ are negligible and will not be produced here. Note that in Eq. (2-10), $\Gamma'_{mg} = \Gamma_{mg} + 1/T_1$, $\Gamma''_{mg} = \Gamma_{mg} + 1/T_2$, and $\Gamma'_{kg} = \Gamma_{kg} + 1/T_1 + 1/T_2$.

From Eq. (2-10) we can see why the SFG is a surface-sensitive experiment. It shows that $\chi^{(2)}_{\alpha\beta\gamma}(\omega_1+\omega_2)$ varies with transition moments in the product form of $\mu_{gk}(\alpha)\mu_{mg}(\beta)\mu_{km}(\gamma)$ etc. which in turn varies with Cartesian coordinates as x^3, x^2y, xyz etc and the spatial averages of these Cartesian cubic products vanish. This indicates that the signal of $\chi^{(2)}_{\alpha\beta\gamma}(\omega_1+\omega_2)$ in the bulk of liquids is zero. Similarly from Eq. (2-10) we can see that a molecular system with the inversion symmetry is SFG forbidden.

Taking the term $\mu_{gk}(\alpha)\mu_{km}(\gamma)\mu_{mg}(\beta)$ as an example, if the state g in $\mu_{gk}(\alpha)$ is of "gerade" symmetry, the k should be "un-gerade". Similarly the state m in $\mu_{km}(\gamma)$ would be "gerade". It follows that $\mu_{mg}(\beta)$ would vanish because of the "gerade" to "gerade" transition in $\mu_{mg}(\beta)$.

As discussed in previous papers, there are four cases of SFG.[17-23] They are resonance–off-resonance, off-resonance–resonance, resonance–resonance, and off-resonance–off-resonance cases. It should be noted that Eq. (2-10) plays the role of the master equation for $\chi^{(2)}_{\alpha\beta\gamma}(\omega_1+\omega_2)$ which can be used to derive the various kinds of SFG spectroscopies.

VIBRATIONAL SUM-FREQUENCY GENERATION

A. Resonance–Off-Resonance Case

In this case (shown in Fig. 2), from Eq. (2-10) we obtain the dominating terms

$$\chi^{(2)}_{\alpha\beta\gamma}(\omega_1+\omega_2)=\frac{i}{\hbar^2}\sum_g\sum_m\Delta\sigma(gm)\frac{\mu_{mg}(\beta)}{i(\omega_{mg}-\omega_1)+\Gamma'_{mg}}\times\sum_k\left[\frac{\mu_{gk}(\alpha)\mu_{km}(\gamma)}{\omega_{kg}-\omega_1-\omega_2}+\frac{\mu_{km}(\alpha)\mu_{gk}(\gamma)}{\omega_{km}+\omega_1+\omega_2}\right] \quad (3\text{-}1)$$

For vibrational SFG, we have to make the following changes due to the use of the Born-Oppenheimer approximation, $g\to gv, m\to gv', k\to ku$, i.e., in terms of vibronic states. The ground state and excited states are expressed as $\Psi_{gv}=\Phi_g\Theta_{gv}$ and $\Psi_{ku}=\Phi_k\Theta_{ku}$, respectively. Here, $\Phi_g(\Phi_k)$ denotes the ground (k-th electronic excited) BO wavefunction, and $\Theta_{gv}(\Theta_{ku})$ denotes the vibrational wavefunction in the ground (k-th electronic excited) state. It follows that

$$\chi^{(2)}_{\alpha\beta\gamma}(\omega_1+\omega_2)=\frac{i}{\hbar^2}\sum_v\sum_{v'}\Delta\sigma(gv,gv')\frac{\mu_{gv',gv}(\beta)}{i(\omega_{gv',gv}-\omega_1)+\Gamma'_{gv',gv}}\times\sum_{ku}\left[\frac{\mu_{gv,ku}(\alpha)\mu_{ku,gv'}(\gamma)}{\omega_{ku,gv}-\omega_1-\omega_2}+\frac{\mu_{ku,gv'}(\alpha)\mu_{gv,ku}(\gamma)}{\omega_{ku,gv'}+\omega_1+\omega_2}\right] \quad (3\text{-}2)$$

Using the Placzek approximation,[24] $\omega_{ku,gv}-\omega_1-\omega_2\cong\omega_{kg}-\omega_1-\omega_2$, $\omega_{ku,gv}+\omega_1+\omega_2\cong\omega_{kg}+\omega_1+\omega_2$ and

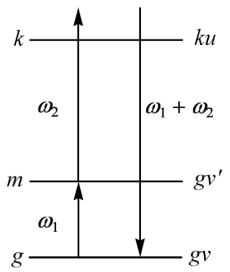

Fig. 2. Energy level diagram for resonance–off-resonance SFG.

$\left(\sum_u|\Theta_{ku}\rangle\langle\Theta_{ku}|\right)=1$, we obtain

$$\chi^{(2)}_{\alpha\beta\gamma}(\omega_1+\omega_2)=\frac{i}{\hbar^2}\sum_v\sum_{v'}\Delta\sigma(gv,gv')\frac{\langle\Theta_{gv'}|\mu_{gg}(\beta)|\Theta_{gv}\rangle}{i(\omega_{gv',gv}-\omega_1)+\Gamma'_{gv',gv}}\times\left\langle\Theta_{gv}\left|\sum_k\left[\frac{\mu_{gk}(\alpha)\mu_{kg}(\gamma)}{\omega_{kg}-\omega_1-\omega_2}+\frac{\mu_{gk}(\gamma)\mu_{kg}(\alpha)}{\omega_{kg}+\omega_1+\omega_2}\right]\right|\Theta_{gv'}\right\rangle \quad (3\text{-}3)$$

or

$$\chi^{(2)}_{\alpha\beta\gamma}(\omega_1+\omega_2)=\frac{i}{\hbar^2}\sum_v\sum_{v'}\Delta\sigma(gv,gv')\times\frac{\langle\Theta_{gv'}|\mu_{gg}(\beta)|\Theta_{gv}\rangle}{i(\omega_{gv',gv}-\omega_1)+\Gamma'_{gv',gv}}\langle\Theta_{gv}|\alpha_{gg}(\alpha\gamma)|\Theta_{gv'}\rangle \quad (3\text{-}4)$$

where $\alpha_{gg}(\alpha\gamma)$ denotes the polarizability of the g electronic state,

$$\alpha_{gg}(\alpha\gamma)=\sum_k\left[\frac{\mu_{gk}(\alpha)\mu_{kg}(\gamma)}{\omega_{kg}-\omega_1-\omega_2}+\frac{\mu_{gk}(\gamma)\mu_{kg}(\alpha)}{\omega_{kg}+\omega_1+\omega_2}\right] \quad (3\text{-}5)$$

Both $\alpha_{gg}(\alpha\gamma)$ and $\mu_{gg}(\beta)$ should be expanded in terms of normal coordinates Q_l,

$$\mu_{gg}(\beta)=\mu^0_{gg}(\beta)+\sum_l\left(\frac{\partial\mu_{gg}(\beta)}{\partial Q_l}\right)_0Q_l+\cdots \quad (3\text{-}6)$$

and

$$\alpha_{gg}(\alpha\gamma)=\alpha^0_{gg}(\alpha\gamma)+\sum_l\left(\frac{\partial\alpha_{gg}(\alpha\gamma)}{\partial Q_l}\right)_0Q_l+\cdots \quad (3\text{-}7)$$

Substituting Eqs. (3-6) and (3-7) into Eq. (3-4) yields

$$\chi^{(2)}_{\alpha\beta\gamma}(\omega_1+\omega_2)=i\sum_v\sum_{v'}\sum_lK_l(\omega_1,\omega_2)\Delta\sigma(gv,gv')\frac{\left|\langle\Theta_{gv}|Q_l|\Theta_{gv'}\rangle\right|^2}{i(\omega_{gv',gv}-\omega_1)+\Gamma'_{gv',gv}} \quad (3\text{-}8)$$

where

$$K_l(\omega_1,\omega_2)=\frac{1}{\hbar^2}\left(\frac{\partial\mu_{gg}(\beta)}{\partial Q_l}\right)_0\left(\frac{\partial\alpha_{gg}(\alpha\gamma)}{\partial Q_l}\right)_0 \quad (3\text{-}9)$$

This indicates that for this vibrational SFG to be non-zero, we should have

$$\left(\frac{\partial\mu_{gg}(\beta)}{\partial Q_l}\right)_0\neq0 \quad (3\text{-}10)$$

and

$$\left(\frac{\partial\alpha_{gg}(\alpha\gamma)}{\partial Q_l}\right)_0\neq0 \quad (3\text{-}11)$$

That is, the Q_l mode should be both IR and Raman active.

In early IR-Vis/UV SFG experiments only $\left|\chi^{(2)}\right|^2$

could be obtained from SFG signal intensities. Neither Re[$\chi^{(2)}$] nor Im[$\chi^{(2)}$] could be measured directly; they were fitted from $\left|\chi^{(2)}\right|^2$ profiles and might yield significantly different interpretation.[25] In 1990 Superfine et al. tried to determine the "absolute phase" of second-order susceptibility by investigating the relative sign of dipole moment derivative and polarizability derivative with respect to the vibrational normal mode.[26,27] This technique became mature in the 2000s and was applied to the water interface geometry.[25,28]

To take into account the phase effect on SFG, we shall rewrite $\chi^{(2)}_{\alpha\beta\gamma}(\omega_1+\omega_2)$ as follows

$$\chi^{(2)}_{\alpha\beta\gamma}(\omega_1+\omega_2)=\chi^{(2)}_{\alpha\beta\gamma}(\omega_1+\omega_2)_R+i\chi^{(2)}_{\alpha\beta\gamma}(\omega_1+\omega_2)_I \quad (3\text{-}12)$$

where

$$\chi^{(2)}_{\alpha\beta\gamma}(\omega_1+\omega_2)_R=\sum_v\sum_{v'}\sum_l K_l(\omega_1,\omega_2)\Delta\sigma(gv,gv')\times\frac{(\omega_{gv',gv}-\omega_1)\left|\langle\Theta_{gv}|Q_l|\Theta_{gv'}\rangle\right|^2}{(\omega_{gv',gv}-\omega_1)^2+\Gamma'^2_{gv',gv}} \quad (3\text{-}13)$$

and

$$\chi^{(2)}_{\alpha\beta\gamma}(\omega_1+\omega_2)_I=\sum_v\sum_{v'}\sum_l K_l(\omega_1,\omega_2)\Delta\sigma(gv,gv')\frac{\Gamma'_{gv',gv}\left|\langle\Theta_{gv}|Q_l|\Theta_{gv'}\rangle\right|^2}{(\omega_{gv',gv}-\omega_1)^2+\Gamma'^2_{gv',gv}} \quad (3\text{-}14)$$

Notice that $\chi^{(2)}_{\alpha\beta\gamma}(\omega_1+\omega_2)_R$ and $\chi^{(2)}_{\alpha\beta\gamma}(\omega_1+\omega_2)_I$ satisfy the Kramers-Kroning relation.

In the following we shall use an example to show how to calculate the vibrational SFG spectra by using the quantum chemical calculations. Graphene is a novel material due to its unique geometric structure and hence related properties such as electric potential, conductivity, etc. It raises interest as well in the adsorption behavior of this substrate, e.g. the orientations of organic polymers adsorbed on the graphene surface, and people have initiated SFG experiments to study this topic.[29] From the theoretical point of view, we have carried out a preliminary SFG simulation of styrene–graphene adsorption system.[30]

In our approach, the first step was to construct molecular models of ethylbenzene, styrene monomer, and polymerized styrene oligomers (up to 4 units) adsorbed on a (finite-sized) graphene sheet. It was followed by geometric optimization of styrene molecules by DFT computations and it showed the phenyl groups tended to "stand" rather than "lay down" on the graphene surface. With calculated dipole derivatives and polarizability derivatives the vibrational SFG spectra of phenyl and alkyl CH stretching modes were simulated with different polarization combinations. These results, some of which are demonstrated in Figs. 3 and 4, have provided the first theoretical prediction to the graphene-based adsorption system and are waiting for experimental investigation.

B. Double-Resonance Case I

In this case (see Fig. 5), from Eq. (2-10) we find

$$\chi^{(2)}_{\alpha\beta\gamma}(\omega_1+\omega_2)=\frac{i^2}{\hbar^2}\sum_g\sum_m\Delta\sigma(gm)\times\sum_k\frac{\mu_{gk}(\alpha)\mu_{mg}(\beta)\mu_{km}(\gamma)}{\left[i(\omega_{mg}-\omega_1)+\Gamma'_{mg}\right]\left[i(\omega_{kg}-\omega_1-\omega_2)+\Gamma'_{kg}\right]} \quad (3\text{-}15)$$

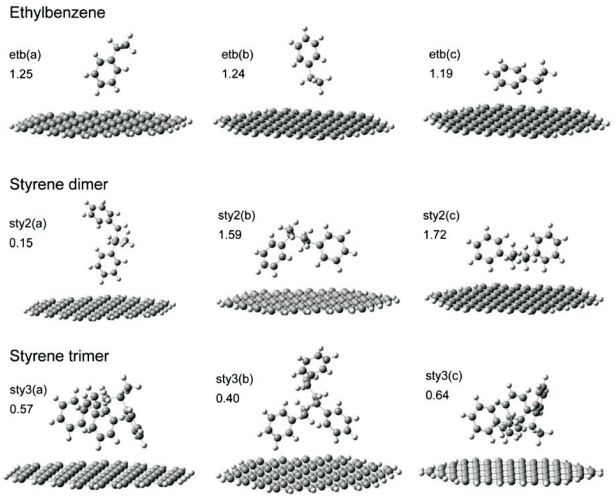

Fig. 3. Optimized structures and stabilization energies (in kcal/mol) of ethylbenzene–graphene and styrene oligomer–graphene systems calculated by B3LYP/6-31G(d). Adopted from Ref. 30.

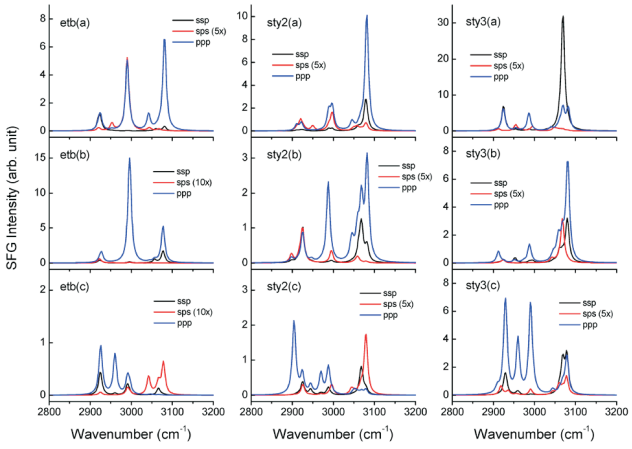

Fig. 4. Simulated SFG spectra of ethylbenzene– and styrene-oligomer–graphene systems. The corresponding conformers are shown in Fig. 3. Adopted from Ref. 30.

In the adiabatic approximation, Eq. (3-15) can be written as

$$\chi^{(2)}_{\alpha\beta\gamma}(\omega_1+\omega_2)=\frac{i^2}{\hbar^2}\sum_v\sum_{v'}\Delta\sigma(gv,gv')\times\sum_u\frac{\mu_{gv,ku}(\alpha)\mu_{gv',gv}(\beta)\mu_{ku,gv'}(\gamma)}{\left[i\left(\omega_{gv',gv}-\omega_1\right)+\Gamma'_{gv',gv}\right]\left[i\left(\omega_{ku,gv}-\omega_1-\omega_2\right)+\Gamma'_{ku,gv}\right]} \quad (3\text{-}16)$$

or

$$\chi^{(2)}_{\alpha\beta\gamma}(\omega_1+\omega_2)=\frac{i^2}{\hbar^2}\sum_v\sum_{v'}\Delta\sigma(gv,gv')\frac{\langle\Theta_{gv'}|\mu_{gg}(\beta)|\Theta_{gv}\rangle}{i\left(\omega_{gv',gv}-\omega_1\right)+\Gamma'_{gv',gv}}\times\left[\sum_u\frac{\langle\Theta_{gv}|\mu_{gk}(\alpha)|\Theta_{ku}\rangle\langle\Theta_{ku}|\mu_{kg}(\gamma)|\Theta_{gv'}\rangle}{i\left(\omega_{ku,gv}-\omega_1-\omega_2\right)+\Gamma'_{ku,gv}}\right] \quad (3\text{-}17)$$

This implies that this type of SFG consists of the IR and resonance Raman scattering,

$$\chi^{(2)}_{\alpha\beta\gamma}(\omega_1+\omega_2)=\frac{i^2}{\hbar^2}\sum_v\sum_{v'}\sum_l\Delta\sigma(gv,gv')\frac{\left(\frac{\partial\mu_{gg}(\beta)}{\partial Q_l}\right)_0\langle\Theta_{gv'}|Q_l|\Theta_{gv}\rangle}{i\left(\omega_{gv',gv}-\omega_1\right)+\Gamma'_{gv',gv}}\times\left[\sum_u\frac{\langle\Theta_{gv}|\mu_{gk}(\alpha)|\Theta_{ku}\rangle\langle\Theta_{ku}|\mu_{kg}(\gamma)|\Theta_{gv'}\rangle}{i\left(\omega_{ku,gv}-\omega_1-\omega_2\right)+\Gamma'_{ku,gv}}\right] \quad (3\text{-}18)$$

or in the Condon approximation,

$$\chi^{(2)}_{\alpha\beta\gamma}(\omega_1+\omega_2)=\frac{i^2}{\hbar^2}\mu^0_{gk}(\alpha)\mu^0_{kg}(\gamma)\sum_v\sum_{v'}\sum_l\Delta\sigma(gv,gv')\times\frac{\left(\frac{\partial\mu_{gg}(\beta)}{\partial Q_l}\right)_0\langle\Theta_{gv'}|Q_l|\Theta_{gv}\rangle}{i\left(\omega_{gv',gv}-\omega_1\right)+\Gamma'_{gv',gv}}\left[\sum_u\frac{\langle\Theta_{gv}|\Theta_{ku}\rangle\langle\Theta_{ku}|\Theta_{gv'}\rangle}{i\left(\omega_{ku,gv}-\omega_1-\omega_2\right)+\Gamma'_{ku,gv}}\right] \quad (3\text{-}19)$$

where μ should be expanded in terms of normal coordinates Q_l, taking $\mu_{gk}(\alpha)$ as an example,

$$\mu_{gk}(\alpha)=\mu^0_{gk}(\alpha)+\sum_l\left(\frac{\partial\mu_{gk}(\alpha)}{\partial Q_l}\right)_0Q_l+\cdots \quad (3\text{-}20)$$

The experiment for doubly resonant IR-Vis SFG has been developed by Shen et al[19,20] and applied to Rhodamin 6G on silica surfaces. This SFG is basically a two-dimensional surface spectroscopy. Given a ω_{Vis} (or λ_{Vis}), the intensity of SFG spectra versus ω_{IR} is shown in Fig. 6 and given a ω_{IR} (or λ_{IR}) the intensity of SFG spectra versus ω_{Vis} (or λ_{Vis}) is shown in Fig. 7. The theoretically calculated SFG spectra are also shown for comparison. For convenience, the absorption spectra of Rhodamin 6G is shown in Fig. 8.

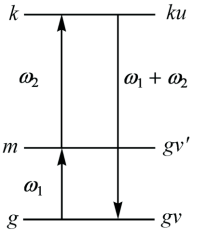

Fig. 5. Energy level diagram for double resonance SFG.

C. Double-Resonance Case II

In this case (see Fig. 9), from Eq. (2-10) we find that Eq. (3-15) can be used with the adiabatic approximation $g\to gv, m\to mu, k\to mu'$ to obtain

$$\chi^{(2)}_{\alpha\beta\gamma}(\omega_1+\omega_2)=\frac{i^2}{\hbar^2}\sum_v\sum_u\Delta\sigma(gv,mu)\times\sum_{u'}\frac{\mu_{gv,mu'}(\alpha)\mu_{mu',gv}(\beta)\mu_{mu',mu}(\gamma)}{\left[i\left(\omega_{mu,gv}-\omega_1\right)+\Gamma'_{mu,gv}\right]\left[i\left(\omega_{mu',gv}-\omega_1-\omega_2\right)+\Gamma'_{mu',gv}\right]} \quad (3\text{-}21)$$

It should be noted that this vibrational SFG can provide us the vibrational information of the excited electronic *m* state, if we fix ω_1 and vary ω_2. On the other hand, if we fix ω_2 and vary ω_1, we can also get the vibrational information of the *m* excited electronic state through the vibronic spectra of the *m* state.

ELECTRONIC SUM-FREQUENCY GENERATION

A. Resonance–Off-Resonance Case

In this case (see Fig. 10), from Eq. (2-10) we obtain

$$\chi^{(2)}_{\alpha\beta\gamma}(\omega_1+\omega_2)=\frac{i}{\hbar^2}\sum_g\sum_m\Delta\sigma(gm)\frac{\mu_{mg}(\beta)}{i\left(\omega_{mg}-\omega_1\right)+\Gamma'_{mg}}\times\sum_k\left[\frac{\mu_{gk}(\alpha)\mu_{km}(\gamma)}{\omega_{kg}-\omega_1-\omega_2}+\frac{\mu_{km}(\alpha)\mu_{gk}(\gamma)}{\omega_{km}+\omega_1+\omega_2}\right] \quad (4\text{-}1)$$

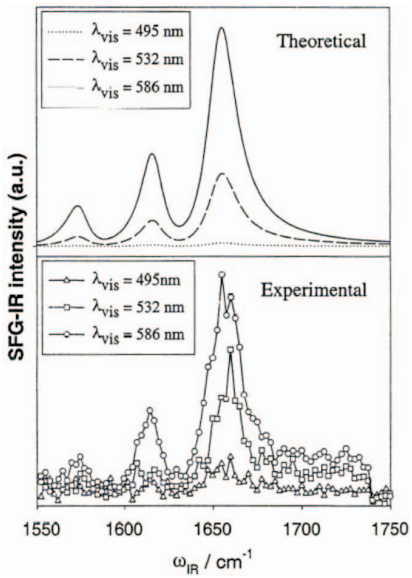

Fig. 6. Double resonant SFG spectra for Rhodmin 6G with a fixed ω_{Vis} (or λ_{Vis}).

For electronic SFG, we have to make the following changes due to the use of the Born-Oppenheimer approximation,

$$g \to gv,\ m \to mu,\ k \to kw$$

where *gv*, *mu* and *kw* denote the vibronic states. It follows that

$$\chi^{(2)}_{\alpha\beta\gamma}(\omega_1+\omega_2)=\frac{i}{\hbar^2}\sum_{v}\sum_{mu}\Delta\sigma(gv,mu)\frac{\mu_{mu,gv}(\beta)}{i(\omega_{mu,gv}-\omega_1)+\Gamma'_{mg}} \times\sum_{kw}\left[\frac{\mu_{gv,kw}(\alpha)\mu_{kw,mu}(\gamma)}{\omega_{kw,gv}-\omega_1-\omega_2}+\frac{\mu_{kw,mu}(\alpha)\mu_{gv,kw}(\gamma)}{\omega_{kw,mu}+\omega_1+\omega_2}\right] \quad (4\text{-}2)$$

By using the Placzek approximation[24] and the closure relation $\sum_{w}|kw\rangle\langle kw|=1$, we obtain,

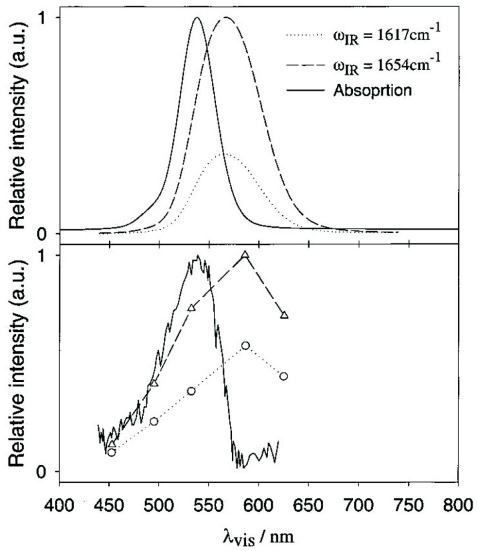

Fig. 7. Double resonant SFG spectra for Rhodmin 6G with a fixed ω_{IR} (or λ_{IR}).

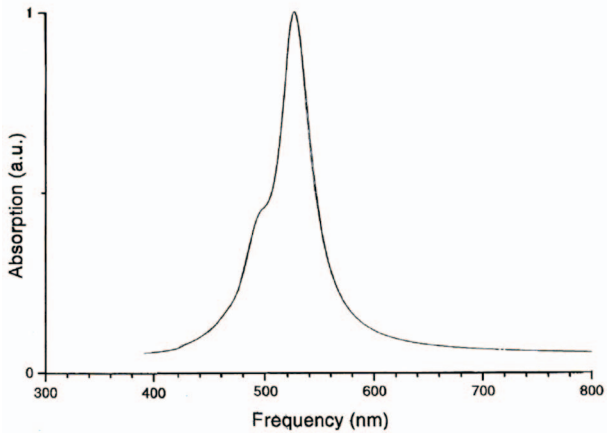

Fig. 8. Absorption spectra of Rhodmin 6G.

$$\chi^{(2)}_{\alpha\beta\gamma}(\omega_1+\omega_2)=\frac{i}{\hbar^2}\sum_{v}\sum_{mu}\Delta\sigma(gv,mu)\frac{\langle\Theta_{mu}|\mu_{mg}(\beta)|\Theta_{gv}\rangle}{i(\omega_{mu,gv}-\omega_1)+\Gamma'_{mg}} \times\sum_{kw}\left[\frac{\langle\Theta_{mu}|\mu_{gk}(\alpha)\mu_{km}(\gamma)|\Theta_{gv}\rangle}{\omega_{kw,gv}-\omega_1-\omega_2}+\frac{\langle\Theta_{mu}|\mu_{gk}(\gamma)\mu_{km}(\alpha)|\Theta_{gv}\rangle}{\omega_{kw,mu}+\omega_1+\omega_2}\right] \quad (4\text{-}3)$$

or

$$\chi^{(2)}_{\alpha\beta\gamma}(\omega_1+\omega_2)=\frac{i}{\hbar^2}\sum_{v}\sum_{mu}\Delta\sigma(gv,mu) \times\sum_{kw}\frac{\langle\Theta_{mu}|\mu_{mg}(\beta)|\Theta_{gv}\rangle\langle\Theta_{gv}|\alpha_{gm}(\alpha\gamma)|\Theta_{mu}\rangle}{i(\omega_{mu,gv}-\omega_1)+\Gamma'_{mg}} \quad (4\text{-}4)$$

where

$$\alpha_{gm}(\alpha\gamma)=\sum_{k}\left[\frac{\mu_{gk}(\alpha)\mu_{km}(\gamma)}{\omega_{kg}-\omega_1-\omega_2}+\frac{\mu_{gk}(\gamma)\mu_{km}(\alpha)}{\omega_{km}+\omega_1+\omega_2}\right] \quad (4\text{-}5)$$

Notice that

$$\chi^{(2)}_{\alpha\beta\gamma}(\omega_1+\omega_2)=\chi^{(2)}_{\alpha\beta\gamma}(\omega_1+\omega_2)_R+i\chi^{(2)}_{\alpha\beta\gamma}(\omega_1+\omega_2)_I \quad (4\text{-}6)$$

where the real part is

$$\chi^{(2)}_{\alpha\beta\gamma}(\omega_1+\omega_2)_R=\frac{1}{\hbar^2}\sum_{v}\sum_{u}\Delta\sigma(gv,mu) \times\frac{(\omega_{mu,gv}-\omega_1)\langle\Theta_{mu}|\mu_{mg}(\beta)|\Theta_{gv}\rangle\langle\Theta_{gv}|\alpha_{gm}(\alpha\gamma)|\Theta_{mu}\rangle}{(\omega_{mu,gv}-\omega_1)^2+\Gamma'^2_{mu,gv}} \quad (4\text{-}7)$$

and the imaginary part is

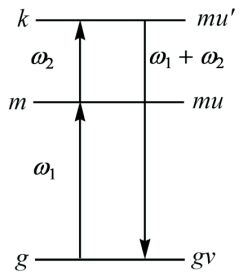

Fig. 9. Energy level diagram for double resonance SFG.

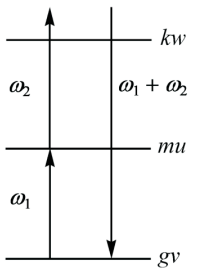

Fig. 10. Energy level diagram for resonance–off-resonance electronic SFG.

$$\chi^{(2)}_{\alpha\beta\gamma}(\omega_1+\omega_2)_I=\frac{1}{\hbar^2}\sum_v\sum_u\Delta\sigma(gv,mu)\times\frac{\Gamma'_{mu,gv}\langle\Theta_{mu}|\mu_{mg}(\beta)|\Theta_{gv}\rangle\langle\Theta_{gv}|\alpha_{gm}(\alpha\gamma)|\Theta_{mu}\rangle}{(\omega_{mu,gv}-\omega_1)^2+\Gamma'^2_{mu,gv}} \quad (4\text{-}8)$$

Eq. (4-8) indicates that the imaginary part of $\chi^{(2)}_{\alpha\beta\gamma}(\omega_1+\omega_2)$ is closely related to the electronic absorption spectra.

In the Condon approximation we obtain

$$\chi^{(2)}_{\alpha\beta\gamma}(\omega_1+\omega_2)_R=\frac{1}{\hbar^2}\mu^0_{mg}(\beta)\alpha^0_{gm}(\alpha\gamma)\sum_v\sum_u\Delta\sigma(gv,mu)\times\frac{(\omega_{mu,gv}-\omega_1)\langle\Theta_{gv}|\Theta_{mu}\rangle^2}{(\omega_{mu,gv}-\omega_1)^2+\Gamma'^2_{mu,gv}} \quad (4\text{-}9)$$

and

$$\chi^{(2)}_{\alpha\beta\gamma}(\omega_1+\omega_2)_I=\frac{1}{\hbar^2}\mu^0_{mg}(\beta)\alpha^0_{gm}(\alpha\gamma)\sum_v\sum_u\Delta\sigma(gv,mu)\times\frac{\Gamma'_{mu,gv}|\langle\Theta_{gv}|\Theta_{mu}\rangle|^2}{(\omega_{mu,gv}-\omega_1)^2+\Gamma'^2_{mu,gv}} \quad (4\text{-}10)$$

Notice that

$$\alpha^0_{gm}(\alpha\gamma)=\sum_k\left[\frac{\mu^0_{gk}(\alpha)\mu^0_{km}(\gamma)}{\omega_{kg}-\omega_1-\omega_2}+\frac{\mu^0_{gk}(\gamma)\mu^0_{km}(\alpha)}{\omega_{kg}+\omega_{gm}+\omega_1+\omega_2}\right] \quad (4\text{-}11)$$

The $g\leftrightarrow m$ transition intensity in electronic SFG is determined by the electronic matrix element $\mu_{mg}(\beta)\alpha_{gm}(\alpha\gamma)$ rather than $|\vec{\mu}_{mg}|^2$ in the ordinary absorption spectra.

B. Off-Resonance–Resonance Case

We next consider the off-resonance–resonance case (shown in Fig. 11). From Eq. (2-10) we find

$$\chi^{(2)}_{\alpha\beta\gamma}(\omega_1+\omega_2)=\frac{i}{\hbar^2}\sum_g\sum_k\sum_m\Delta\sigma(gm)\times\frac{\mu_{gk}(\alpha)}{i(\omega_{kg}-\omega_1-\omega_2)+\Gamma'_{kg}}\left[\frac{\mu_{mg}(\beta)\mu_{km}(\gamma)}{\omega_{mg}-\omega_1}+\frac{\mu_{mg}(\gamma)\mu_{km}(\beta)}{\omega_{mg}-\omega_2}\right] \quad (4\text{-}12)$$

In terms of vibronic states, we find (with the Placzek approximation $\omega_{mu,gv}\approx\omega_{mg}$)

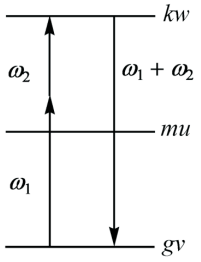

Fig. 11. Energy level diagram for off-resonance–resonance electronic SFG.

$$\chi^{(2)}_{\alpha\beta\gamma}(\omega_1+\omega_2)=\frac{i}{\hbar^2}\sum_v\sum_w\sum_m\Delta\sigma(gv,mu)\frac{\langle\Theta_{gv}|\mu_{gk}(\alpha)|\Theta_{kw}\rangle}{i(\omega_{kw,gv}-\omega_1-\omega_2)+\Gamma'_{kw,gv}}\times\left[\frac{\langle\Theta_{kw}|\mu_{km}(\gamma)\mu_{mg}(\beta)|\Theta_{kw}\rangle}{\omega_{mg}-\omega_1}+\frac{\langle\Theta_{kw}|\mu_{km}(\beta)\mu_{mg}(\gamma)|\Theta_{gv}\rangle}{\omega_{mg}-\omega_2}\right] \quad (4\text{-}13)$$

or

$$\chi^{(2)}_{\alpha\beta\gamma}(\omega_1+\omega_2)=\frac{i}{\hbar^2}\sum_v\sum_w\Delta\sigma(gv,mu)\times\frac{\langle\Theta_{gv}|\mu_{gk}(\alpha)|\Theta_{kw}\rangle\langle\Theta_{kw}|\alpha_{kg}(\beta\gamma)|\Theta_{gv}\rangle}{i(\omega_{kw,gv}-\omega_1-\omega_2)+\Gamma'_{kw,gv}} \quad (4\text{-}14)$$

where

$$\alpha_{kg}(\beta\gamma)=\sum_m\left[\frac{\mu_{km}(\gamma)\mu_{mg}(\beta)}{\omega_{mg}-\omega_1}+\frac{\mu_{km}(\beta)\mu_{mg}(\gamma)}{\omega_{mg}-\omega_2}\right] \quad (4\text{-}15)$$

In the Condon approximation we find that

$$\chi^{(2)}_{\alpha\beta\gamma}(\omega_1+\omega_2)=\chi^{(2)}_{\alpha\beta\gamma}(\omega_1+\omega_2)_R+i\chi^{(2)}_{\alpha\beta\gamma}(\omega_1+\omega_2)_I \quad (4\text{-}16)$$

$$\chi^{(2)}_{\alpha\beta\gamma}(\omega_1+\omega_2)_R=\frac{1}{\hbar^2}\mu^0_{gk}(\alpha)\alpha^0_{kg}(\beta\gamma)\sum_v\sum_w\Delta\sigma(gv,mu)\times\frac{(\omega_{kw,gv}-\omega_1-\omega_2)\langle\Theta_{kw}|\Theta_{gv}\rangle^2}{(\omega_{kw,gv}-\omega_1-\omega_2)^2+\Gamma'^2_{kw,gv}} \quad (4\text{-}17)$$

and

$$\chi^{(2)}_{\alpha\beta\gamma}(\omega_1+\omega_2)_I=\frac{1}{\hbar^2}\mu^0_{gk}(\alpha)\alpha^0_{kg}(\beta\gamma)\sum_v\sum_w\Delta\sigma(gv,mu)\times\frac{\Gamma'_{kw,gv}|\langle\Theta_{kw}|\Theta_{gv}\rangle|^2}{(\omega_{kw,gv}-\omega_1-\omega_2)^2+\Gamma'^2_{kw,gv}} \quad (4\text{-}18)$$

$\chi^{(2)}_{\alpha\beta\gamma}(\omega_1+\omega_2)_I$ shows that it is closely related to the absorption spectra for the electronic transition $g\rightarrow k$ with the sum frequency $\omega_1+\omega_2$.

In addition to VSFG, Tahara and co-workers have recently made heterodyne-detected electronic sum-frequency generation (ESFG) applicable.[10-12] In their experiments, two visible/near-infrared beams, one was 795 nm and the other was tunable between 540 nm and 1.2 μm, were guided to the sample where the sum frequency was tuned resonant with an electronic state. By this means they have resolved the orientation of surfactant-like molecules floating on water surface.[13] Following that they have studied the pH spectrometry of an air/cationic surfactant/water interface by the same technique, obtaining an insight to the acid-base equilibrium,[14] and furthermore, to the pH value of water surface, where the value is lower than the bulk by 1.7.[15] It turns out that electronic SFG is helpful to solve this

long-debated issue; however, it should be noticed that a solid theoretical framework to interpret these excellent experimental results is still in demand.

We have chosen 4-methyl-7-hydroxycoumarin (MHC), a pH-indicator surfactant molecule analogous to which Tahara's group used in their experiments,[15] to provide a theoretical support to ESFG spectroscopy. A loose optimization showed that the MHC molecule tends to float on the water surface (simulated by a cluster of ~50 water molecules) with its oxygen atoms immersed into water while methyl group pointing outward (Fig. 12). Under the off-resonance–resonance scheme, the dominant transition occurred from the ground state ($1\,^1A'$) to the first excited state ($2\,^1A'$). The corresponding transition dipole moments, two-photon matrix elements, and Franck-Condon integrals were calculated according to Eqs. (4-16) to (4-18) and the SFG spectrum was then simulated (Fig. 13). This preliminary result is the first theoretical ESFG spectrum to our knowledge, and it may be further improved by including more detailed factors like non-Condon contributions, more definite orientation distributions, and explicit solvent effects.

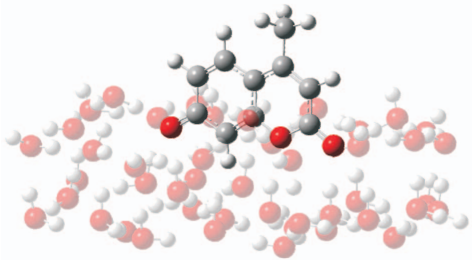

Fig. 12. MHC anion floating on the surface of a small water cluster, where red and dark gray spheres represent oxygen and carbon atoms, respectively.

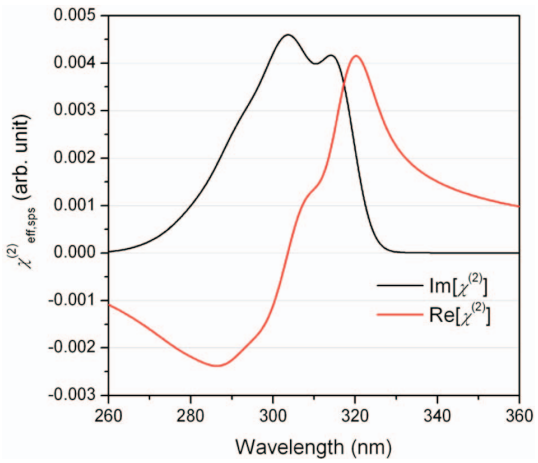

Fig. 13. Simulated electronic SFG spectrum of MHC with the sps polarization.

C. Double Resonance Case

Next we consider the double resonance case (see Fig. 14). From Eq. (2-10) we obtain

$$\chi^{(2)}_{\alpha\beta\gamma}(\omega_1+\omega_2)=\frac{i^2}{\hbar^2}\sum_v\sum_{mu}\sum_{kw}\Delta\sigma(gv,mu)\mu_{gv,kw}(\alpha)\times\frac{\mu_{mu,gv}(\beta)\mu_{kw,mu}(\gamma)}{\left[i(\omega_{mu,gv}-\omega_1)+\Gamma'_{mu,gv}\right]\left[i(\omega_{kw,gv}-\omega_1-\omega_2)+\Gamma'_{kw,gv}\right]} \quad (4\text{-}19)$$

or

$$\chi^{(2)}_{\alpha\beta\gamma}(\omega_1+\omega_2)=\frac{i^2}{\hbar^2}\sum_v\sum_{mu}\sum_{kw}\Delta\sigma(gv,mu)\times\frac{\langle\Theta_{gv}|\mu_{gk}(\alpha)|\Theta_{kw}\rangle\langle\Theta_{mu}|\mu_{mg}(\beta)|\Theta_{gv}\rangle\langle\Theta_{kw}|\mu_{km}(\gamma)|\Theta_{mu}\rangle}{\left[i(\omega_{mu,gv}-\omega_1)+\Gamma'_{mu,gv}\right]\left[i(\omega_{kw,gv}-\omega_1-\omega_2)+\Gamma'_{kw,gv}\right]} \quad (4\text{-}20)$$

In the Condon approximation,

$$\chi^{(2)}_{\alpha\beta\gamma}(\omega_1+\omega_2)=\frac{i^2}{\hbar^2}\mu^0_{gk}(\alpha)\mu^0_{mg}(\beta)\mu^0_{km}(\gamma)\sum_v\sum_{mu}\sum_{kw}\Delta\sigma(gv,mu)\times\frac{\langle\Theta_{gv}|\Theta_{kw}\rangle\langle\Theta_{mu}|\Theta_{gv}\rangle\langle\Theta_{kw}|\Theta_{mu}\rangle}{\left[i(\omega_{mu,gv}-\omega_1)+\Gamma'_{mu,gv}\right]\left[i(\omega_{kw,gv}-\omega_1-\omega_2)+\Gamma'_{kw,gv}\right]} \quad (4\text{-}21)$$

Notice that

$$\chi^{(2)}_{\alpha\beta\gamma}(\omega_1+\omega_2)=\chi^{(2)}_{\alpha\beta\gamma}(\omega_1+\omega_2)_R+i\chi^{(2)}_{\alpha\beta\gamma}(\omega_1+\omega_2)_I \quad (4\text{-}22)$$

where

$$\chi^{(2)}_{\alpha\beta\gamma}(\omega_1+\omega_2)_R=\frac{i^2}{\hbar^2}\mu^0_{gk}(\alpha)\mu^0_{mg}(\beta)\mu^0_{km}(\gamma)\sum_v\sum_u\sum_w\Delta\sigma(gv,mu)\times\left[-(\omega_{mu,gv}-\omega_1)(\omega_{kw,gv}-\omega_1-\omega_2)+\Gamma'_{mu,gv}\Gamma'_{kw,gv}\right]\times\frac{\langle\Theta_{gv}|\Theta_{kw}\rangle\langle\Theta_{kw}|\Theta_{mu}\rangle\langle\Theta_{mu}|\Theta_{gv}\rangle}{\left[(\omega_{mu,gv}-\omega_1)^2+\Gamma'^2_{mu,gv}\right]\left[(\omega_{kw,gv}-\omega_1-\omega_2)^2+\Gamma'^2_{kw,gv}\right]} \quad (4\text{-}23)$$

and

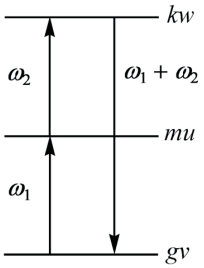

Fig. 14. Energy level diagram for double resonance electronic SFG.

$$\chi^{(2)}_{\alpha\beta\gamma}(\omega_1+\omega_2)_I = \frac{i^2}{\hbar^2}\mu^0_{gk}(\alpha)\mu^0_{mg}(\beta)\mu^0_{km}(\gamma)\sum_v\sum_u\sum_w \Delta\sigma(gv,mu) \times\left[\Gamma'_{mu,gv}(\omega_{kw,gv}-\omega_1-\omega_2)+\Gamma'_{kw,gv}(\omega_{mu,gv}-\omega_1)\right] \times\frac{\langle\Theta_{gv}|\Theta_{kw}\rangle\langle\Theta_{kw}|\Theta_{mu}\rangle\langle\Theta_{mu}|\Theta_{gv}\rangle}{\left[(\omega_{mu,gv}-\omega_1)^2+\Gamma'^2_{mu,gv}\right]\left[(\omega_{kw,gv}-\omega_1-\omega_2)^2+\Gamma'^2_{kw,gv}\right]} \quad (4\text{-}24)$$

ORIENTATION AND EULER ANGLE TRANSFORM

Till now we focused on the second-order susceptibility, $\chi^{(2)}$, of a molecular system embedded in a heat bath. To correlate these molecular properties to experimental observables, one has to include information of molecular orientation distribution as well as beam angles defined under laboratory frames. Given the molecular coordinates, *xyz*, laboratory frames, *XYZ*, and the rotation angles, ϕθψ, in the *z-y-z* convention (Fig. 15), the Euler rotation matrix between the two coordinate systems is [31] angles (ϕθψ) between the two coordinate systems.

$$R=\begin{bmatrix}R_{Xx}&R_{Xy}&R_{Xz}\\R_{Yx}&R_{Yy}&R_{Yz}\\R_{Zx}&R_{Zy}&R_{Zz}\end{bmatrix} =\begin{bmatrix}\cos\phi\cos\theta\cos\psi-\sin\phi\sin\psi&-\cos\phi\cos\theta\sin\psi-\sin\phi\cos\psi&\cos\phi\sin\theta\\\sin\phi\cos\theta\cos\psi+\cos\phi\sin\psi&-\sin\phi\cos\theta\sin\psi+\cos\phi\cos\psi&\sin\phi\sin\theta\\-\sin\theta\cos\psi&\sin\theta\sin\psi&\cos\theta\end{bmatrix} \quad (5\text{-}1)$$

Now we consider the projection of molecular second-order susceptibility onto the laboratory frame. With an orientation average over a group of molecules, the projection is

$$\chi^{(2)}_{IJK}=N\sum_{lmn}\chi^{(2)}_{lmn}\left\langle(\hat{I}\cdot\hat{l})(\hat{J}\cdot\hat{m})(\hat{K}\cdot\hat{n})\right\rangle=N\sum_{lmn}\chi^{(2)}_{lmn}\langle R_{Il}R_{Jm}R_{Kn}\rangle \quad (5\text{-}2)$$

where *I*, *J* and *K* indicate laboratory frames *X*, *Y* and/or *Z*, *l*, *m* and *n* refer to molecular coordinates *x*, *y* and/or *z*, *N* is the density of molecules at the interface, and $\langle\cdots\rangle$ is the orientation average. $\chi^{(2)}_{IJK}$ has 27 elements but most of them vanish supposing the molecules have an azimuthally isotropic distribution on the *XY* plane. For example, a molecule of the C_{2v} point group has only seven elements survived and some of them being mutually dependent after the orientation average:[32]

$$\chi^{(2)}_{ZZZ},\quad \chi^{(2)}_{XXZ}=\chi^{(2)}_{YYZ},\quad \chi^{(2)}_{ZXX}=\chi^{(2)}_{ZXZ}=\chi^{(2)}_{ZYY}=\chi^{(2)}_{YZY}. \quad (5\text{-}3)$$

Next we take beam angles into account. Given θ_1 and θ_2 the incident beam angles and θ_{SFG} the output beam angle with respect to the surface/interface normal, the effective susceptibilities at different combination of beam polarizations (*s* or *p*) are[32]

$$\chi^{(2)}_{eff}(ssp)=\sin\theta_1 L_{YY}(\omega_{SFG})L_{YY}(\omega_2)L_{ZZ}(\omega_1)\chi^{(2)}_{XXZ} \quad (5\text{-}4)$$

$$\chi^{(2)}_{eff}(sps)=\sin\theta_2 L_{YY}(\omega_{SFG})L_{ZZ}(\omega_2)L_{YY}(\omega_1)\chi^{(2)}_{XZX} \quad (5\text{-}5)$$

$$\begin{aligned}\chi^{(2)}_{eff}(ppp)=&\sin\theta_{SFG}\sin\theta_2\sin\theta_1 L_{ZZ}(\omega_{SFG})L_{ZZ}(\omega_2)L_{ZZ}(\omega_1)\chi^{(2)}_{ZZZ}\\&-\cos\theta_{SFG}\cos\theta_2\sin\theta_1 L_{XX}(\omega_{SFG})L_{XX}(\omega_2)L_{ZZ}(\omega_1)\chi^{(2)}_{XXZ}\\&+\sin\theta_{SFG}\cos\theta_2\cos\theta_1 L_{ZZ}(\omega_{SFG})L_{XX}(\omega_2)L_{XX}(\omega_1)\chi^{(2)}_{XZX}\\&-\cos\theta_{SFG}\sin\theta_2\cos\theta_1 L_{XX}(\omega_{SFG})L_{ZZ}(\omega_2)L_{XX}(\omega_1)\chi^{(2)}_{XZX}\end{aligned} \quad (5\text{-}6)$$

where the sequence of beam polarization noted here is ω_{SFG}, ω_2 and ω_1. In above equations *L*'s refer to Fresnel factors which are functions of refractive indices and wavelengths.[32,33]

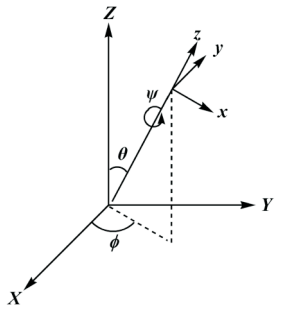

Fig. 15. Cartesian coordinates of laboratory frames (*XYZ*) and molecular axes (*xyz*) and rotation angles (ϕθψ) between the two coordinate systems.

DISCUSSIONS

A. Applications to Water Interface

Faraday was the first to propose that there could exist on ice a thin film of liquid water even below the bulk melting temperature.[34,35] The PPP-SFG vibrational spectra in the OH stretch region for the ice/vapor interface of the hexagonal ice structure exhibit two peaks: the strong peak at ~3200 cm^{-1} that is originated from OH groups hydrogen-bonded to the neighbors and the narrow peak at 3700 cm^{-1} is assigned to the dangling OH bonds at the surface.[36] For the study of surface melting, the orientation information of the dangling OH bonds should provide a clue as to how the peak varies with temperature below the bulk melting temperature. If the ice surface would remain crystalline, the peak position and strength would not change appreciably with temperature. A quantitative analysis of the

peak at 3700 cm^{-1} shows that the orientational order parameter of the dangling OH bonds decreases from 1 (for perfect ordering) around 203 K to 0.3 at 273 K.[36] For water/vapor interface (above 273 K), the orientational order parameter of the dangling OH bonds suggests more ordered orientation compared to quasi-liquid on ice. The SFG-VS spectrum of OH stretch region of the neat water/vapor interface was reported (see Fig. 16).[37] This spectrum has been reproduced by other groups.[38-44] The characteristics of the spectrum are (1) a sharp peak at 3700 cm^{-1} that can be assigned to the dangling OH bonds jutting into the vapor, (2) a very broad band for the hydrogen-bonded OH that can be composed of two sub-bands around 3400 cm^{-1} and 3200 cm^{-1}.[37,45] Comparing these band frequencies to IR absorption bands of bulk ice and liquid samples, it was concluded that OHs in the topmost layer DAA, DDA, and DDAA (Fig. 17, where D and A represent hydrogen donor and hydrogen acceptor, respectively, in the hydrogen-bonding network) molecules loosely donor-bonded to molecules below contributed to the "liquid-like" negative band, while OHs of tetrahedrally bonded DDAA molecules in lower layers contributed to the "ice-like" positive band through their donor-bonding to upper DAA and DDA molecules. This supported the idea that the surface layer of water is relatively disordered, while the lower layers have some ordered (to a certain extent) ice-like structure.[46,47] Many groups have proposed various interpretations of the origin of sub-bands.[39-44,48-54] Thus there has been a great deal of confusion. There have been many theoretical approaches attempting to solve the issue; however it is still difficult to correlate the spectral features with the interfacial structure.[55,56] Another possible reason for the confusion is due to the fact that SFG vibrational spectra were obtained by the intensity proportional to the absolute square of the surface nonlinear susceptibility. The surface nonlinear susceptibility is a complex number and the spectrum of its imaginary part is analogous to the imaginary part of the dielectric function, in other words, that to the absorption or emission spectrum. The phase-sensitive SFG-VS technique developed by Shen's group allows direct observation of the imaginary part of surface nonlinear susceptibility (see Fig. 16).[28,57]

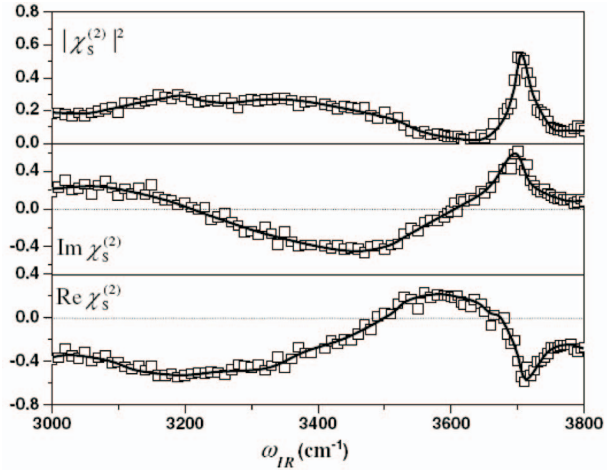

Fig. 16. Phase-sensitive vibrational SFG spectra of water surface in the OH stretching region. Adopted from Ref. 46.

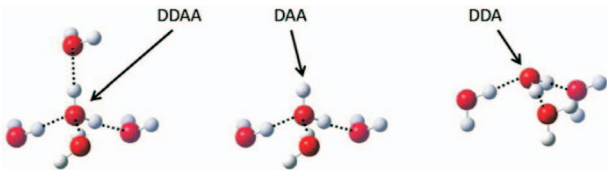

Fig. 17. Configurations of water molecules categorized by hydrogen donating/accepting in the hydrogen-bonding network.

Du et al. was the first to report the fitting result of the measured intensity yielding two negative discrete resonances at 3200 and 3450 cm^{-1}. These two peaks were labeled as "ice-like" (3450 cm^{-1}) and "liquid-like" (3200 cm^{-1}) bands because of their similarities to the IR and Raman spectral features of bulk ice and water.[37,45]

The Richmond group first used two negative and one positive resonance bands for fitting in the bonded-OH region, in addition to one positive and one negative weak shoulder on the two sides of the dangling OH peak.[52] Later, based on isotopic water mixtures results, they fit the bonded-OH part of the H_2O/vapor spectrum by three negative resonance bands at 3200, 3310, and 3420 cm^{-1}, the first two of which were assigned to the donor-bonded OH of the tetrahedral coordination molecules.

Based on the IR and Raman spectral analysis, the Allen group fit the SFG-VS intensity spectrum by three negative resonances bands (3250, 3450 and 3550 cm^{-1}).[40,54] Furthermore, they added a positive peak at 3748 cm^{-1}, which was suggested to be due to two coordination molecules. Wang and co-workers fit the bonded-OH spectrum by three negative resonance bands (3250, 3450, and 3550 cm^{-1}) and different interpretation was made for these three bands.[39,53]

Bonn's group found that the intensity spectrum of the D_2O/vapor interface can be the same as that of H_2O/vapor interface via a frequency rescaling.[43] They fit the bonded-

OD spectrum by two negative resonance bands centered at 2400 and 2515 cm^{-1}. The former corresponds to 3200 cm^{-1} "ice-like" band and the latter to 3400 cm^{-1} "liquid-like" band in the H_2O case. Attribution was made as the symmetric stretch OH mode and its Fermi resonance. Later they fit the intensity spectrum in the bonded-OH region by a different set of bands (one positive band at 2320 cm^{-1} and two negative bands at 2415 and 2540 cm^{-1}). The assignment of the two negative bands was also made in the same way as the previous case.

In short, the fitting spectra of the imaginary part of the second order susceptibility do not show any positive band in the bonded-OH region. However, Shen's group has reported the OH stretch region of the phase-sensitive SFG-VS spectrum of H_2O/vapor and found that the spectrum of the imaginary part of the phase-sensitive SFG-VS consists of roughly three bands: a positive peak at around 3700 cm^{-1}, a negative band from ~ 3200 to 3600 cm^{-1}, and a positive band below 3200 cm^{-1}.[28,57-59] This direct observation result is quite different from those previously reported based on the fitting approaches.

Theoretical calculations on water interfacial structures using MD simulation have been reported over years. There are two types of such simulations: (1) the orientation and geometry of a water molecule in the ensemble are simulated under a given force-field and the coupling matrix elements and normal modes are mapped to those calculated quantum chemistry methods for a given orientation and geometry. In this case, the spectral features can be correlated to the normal modes of a molecule in a certain orientation and geometry. The effects of the intermolecular interaction between the coupling matrix elements are taken into account via constructing the total polarization (or susceptibility) with an electrostatic interaction model,[56] (2) a correlation function of the total dipole moment and total polarizability tensor is generated via MD simulation as a function of the trajectory and the half-Fourier transformation is used to obtain frequency domain spectra.[55] The latter has been popular because of the simplicity of the computational procedure and it allows performing more applications. However, the latter approach does not use any normal modes thus it is quite difficult to correlate the spectral features to the orientation and geometry of a molecule in the ensemble.

With MD simulation approach, strikingly a positive or negative sign of the bands appearing in the resulting spectra depends quite heavily on the type of the force-field used. There seem to be two different mechanisms for the positive band below 3200 cm^{-1}. All MD based simulations calculate the total dipole moment and the total perishability tensor that involve the contribution from all the molecules in the ensemble. Thus when the correlation function is constructed, self-correlation (site correlation) term and interference term appear. The interference term is attributed to the positive band[55,56] while without mentioning these two terms, the different group uses many-body force-field to show a positive band below 3200 cm^{-1}.[60]

Quite recently, quantum MD simulation has been performed on SFG-VS spectra of water/vapor surface,[61] which calculates a potential energy surface quantum mechanically using on-the-fly algorithms. Thus this approach essentially takes into account the many-body effect. Interestingly, only the site-correlation term can produce a positive band below 3200 cm^{-1}. However, due to a time-correlation approach, quantum MD simulation also cannot provide a correlation between the orientation and geometry of the molecule and the spectral features. Understanding of the water/vapor interfacial structure should remain as challenging as to the theorists. It is also important to discuss how the spectrum relates to the interfacial water species.

We would like to treat this problem with a quantum chemical approach based on DAA, DDA, and DDAA configurations. By randomizing orientations and distances of the surrounding three or four molecules, the explicit, averaged dipole and polarizability derivatives of the center water molecule at each configuration could be calculated. The overall simulated SFG spectrum could reproduce detailed features quite well, and the arrangement of report is in the process.[62]

B. Applications to Dye-Sensitized Solar Cells

SFG has also been used to elucidate dye-TiO_2 structure of dye-sensitized solar cells (DSSCs) at the interface.[63-69] Combined both the dye-adsorption geometry information from SFG spectroscopy and the electron transfer dynamics information from ultrafast transient absorption spectroscopy, experimental scientists are able to obtain the detailed information of the correlation between the sensitizer adsorption geometry, electron injection/recombination dynamics, and solar cell performance. For example, to determine whether the electron transfer rates are strongly dependent on spacer and sensitization conditions at molecular level, Ye and coworkers [69] have first applied SFG to the study of the adsorption geometries of the Zn-porphyrin (ZnP) derivatives on the TiO_2 surface and found that the electron transfer between ZnP and TiO_2 occurs "through-

space" rather than "through the molecular spacer" and the sensitization solvent may affect adsorption geometry and adsorption ordering through co-adsorption and modify the electron transfer dynamics and consequently solar cell efficiency.

C. Applications to Biosciences

Since 1996, Vogel demonstrated that the applications of optical harmonic generation and infrared-visible sum frequency generation (SFG) in the biosciences could yield surface specific information concerning, such as molecular adsorption and orientation, surface charges, interfacial hydrogen bond networks, surface chirality, and membrane potentials under *in situ* conditions and with high surface sensitivity.[70] SFG studies on biological interfaces have grown tremendously in recent years.[71-92] For example, using this technique with the combination of the C-H and C=O stretching signals, Chen's group have successfully determined the interfacial structures of membrane-bounded peptides and proteins such as magainin 2, melittin, alamethicin, and G-protein.[75-80] Yan's group have characterized the secondary structures of α-helix, β-sheet, and random-coil at interfaces.[81,82] with 3300 cm^{-1} N-H stretching signal in the SFG spectra, Ye and coworkers have used SFG to study the interfacial protein and peptide absorption.[85-91] With the advantage of *in situ* detection, SFG can be used to characterize low concentrations of different biomolecules such as lipids, peptides and proteins at various interfaces.[93,94]

SFG has been developed as a unique tool to study protein adsorption, which is an important process that occurs on biomedical device surfaces and to investigate effects of protein solution pH and protein interfacial coverage on protein interfacial structures.[95-98] Chen and coworkers have also applied SFG to study isotope labeled proteins for their adsorption for the first time.[99] Accompanied by the developing of the polarization mapping, SFG has also been used to study adsorption behavior of peptides, serving as a model for complicated interfacial proteins and polymers.[86,87,89,100,101] SFG has been proven to be powerful in monitoring the interaction of biomolecules and other small molecules with lipid membranes *in situ*.[76-78,80,81,93,94,102-106] For example, SFG has been applied to investigate the molecular behavior of a novel membrane-active antimicrobial arylamide oligomer 1,[102] and peptides such as melittin,[76] alamethicin,[80] pexiganan (MSI-78),[93] cell penetrating peptide,[94] magainin 2,[103] MSI594,[104] tachyplesin I,[105] and amyloid polypeptide[81,106] in model cell membranes. Recent studies on the peptide alamethicin indicated that when an α-helix connects to a 3_{10}-helix, the 3_{10}-helix itself and that connecting to an α-helix may contribute two peaks centered at 1635 cm^{-1} and 1670 cm^{-1}.[78,80] It is also possible to use SFG to analyze the interaction of large molecules such as proteins with lipids.[77] DNA has also been extensively studied by using SFG. These studies have shown that SFG can provide important structural information of DNA strands at different biological surfaces or interfaces *in situ*.[107-113] Wurpel et al. investigated the DNA interaction with different lipids including 1,2-dipalmitoyl-3-trimethylammonium propane (DPTAP), diC14-amidine and a zwitterionic lipid 1,2-dipalmitoyl-sn-glycero-3-phosphocholine (DPPC) in the presence and absence of calcium ion.[108] Asanuma and coworkers recently investigated the impact of monovalent and divalent metal cations on 20-mer single-stranded DNA (ssDNA) and double-stranded DNA (dsDNA) covalently bound to silicon (111) surface using SFG.[109] Howell et al. chemically immobilized ssDNA on gold substrate via the thiol groups and studied the air–solid, phosphate buffer saline solution (PBS)–solid, and D_2O–solid interfaces.[110] Other SFG studies of DNA,[111,112] including on platinum substrates have also been reported.[113]

Furthermore, recently time dependent SFG has been applied to study molecular kinetics and dynamics on various biomolecules such as peptides and lipids at interfaces. For example, SFG was applied in *in situ* studies of peptide and protein immobilization on surfaces,[114-116] protein adsorption such as fibrinogen to different polymers,[685,117] and to monitor the kinetics of flip-flop process.[118-123] The kinetic studies of flip-flop showed that lipid flip-flop can be affected by chemical structural modifications of lipids[119] and transmembrane peptides such as gramicidin A,[120] WALP23 and melittin,[121] membrane lateral pressure,[122] as well as cholesterol.[123] SFG has also been used to study the time-dependent interactions between peptide and a DPPG bilayer such as melittin[124] and tachyplesin I.[125] These researches show time-dependent SFG is an ideal technique to study many biological interactions involving peptides/proteins and membrane lipid bilayers.

In concluding this paper, we can see that in view of the recent tremendous experimental activities of SFG, quantum chemical calculations of SFG spectra to analyze the experimental SFG spectra are badly needed. Finally, we shall discuss whether it is possible to use SFG as a surface-sensitive technique like SERS (surface-enhanced Raman Scattering). In SERS, it is believed to exist two enhancements, physical one which is due to the electric field

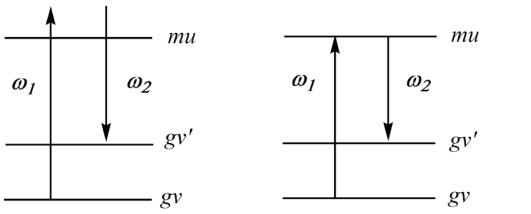

Fig. 18. Energy level diagram for Raman scattering and Resonance-Raman scattering.

enhancement resulting from the geometry of the nano-particle causing the enhancement of the Raman scattering, and chemical one which is due to the creation of charge-transfer bands resulting from the interaction between surface-plasmon and excited electronic states of adsorbed molecules. These charge-transfer bands transform the original Raman spectra into the resonance Raman spectra (see Fig. 18). The similar situation exists for the surface-enhanced SFG. This can be seen from Figs. 2 and 5.

ACKNOWLEGEMENT

The authors wish to thank the National Science Council of Taiwan and National Chiao-Tung University for supporting this project.

REFERENCES

1. Hunt, J. H.; Guyot-Sionnest, P.; Shen, Y. R. *Chem. Phys. Lett.* **1987**, *133*, 189.
2. Guyot-Sionnest, P.; Hunt, J. H.; Shen, Y. R. *Phys. Rev. Lett.* **1987**, *59*, 1597.
3. Chen, Z.; Gracias, D. H.; Somorjai, G. A. *Appl. Phys. B* **1999**, *68*, 549.
4. Gracias, D. H.; Chen, Z.; Shen, Y. R.; Somorjai, G. A. *Acc. Chem. Res.* **1999**, *32*, 930.
5. Briggman, K. A.; Stephenson, J. C.; Wallace, W. E.; Richter, L. J. *J. Phys. Chem. B* **2001**, *105*, 2785.
6. Gautam, K. S.; Schwab, A. D.; Dhinojwala, A.; Zhang, D.; Dougal, S. M.; Yeganeh, M. S. *Phys. Rev. Lett.* **2000**, *85*, 3854.
7. Chen, Z.; Ward, R.; Tian, Y.; Eppler, A. S.; Shen, Y. R.; Somorjai, G. A. *J. Am. Chem. Soc.* **2000**, *122*, 10615.
8. Chen, Z.; Ward, R.; Tian, Y.; Eppler, A. S.; Shen, Y. R.; Somorjai, G. A. *J. Phys. Chem. B* **1999**, *103*, 2935.
9. Wei, X.; Hong, S.-C.; Lvovsky, A. I.; Held, H.; Shen, Y. R. *J. Phys. Chem. B* **2000**, *104*, 3349.
10. Yamaguchi, S.; Tahara, T. *J. Phys. Chem. B* **2004**, *108*, 19079.
11. Yamaguchi, S.; Tahara, T. *J. Chem. Phys.* **2008**, *129*, 101102.
12. Mondal, S. K.; Yamaguchi, S.; Tahara, T. *J. Phys. Chem. C* **2011**, *115*, 3083.
13. Watanabe, H.; Yamaguchi, S.; Sen, S.; Morita, A.; Tahara, T. *J. Chem. Phys.* **2010**, *132*, 144701.
14. Yamaguchi, S.; Bhattacharyya, K.; Tahara, T. *J. Phys. Chem. C* **2011**, *115*, 4168.
15. Yamaguchi, S.; Kundu, A.; Sen, P.; Tahara, T. *J. Chem. Phys.* **2012**, *137*, 151101.
16. Lin, S. H.; Alden, R.; Islampour, R.; Ma, H.; Villaeys, A. A. *Density Matrix Method and Femtosecond Processes*; World Scientific: Singapore, 1991; p 6.
17. Hayashi, M.; Lin, S. H. In *Advances in Multi-photon Processes and Spectroscopy*; Lin, S. H.; Villaeys, A. A.; Fujimura, Y., Eds; World Scientific: Singapore, 2004; Vol. 16, pp 307-422.
18. Hayashi, M.; Lin, S. H.; Shen, Y. R. *J. Phys. Chem. A* **2004**, *108*, 8058.
19. Hayashi, M.; Lin, S. H.; Raschke, M. B.; Shen, Y. R. *J. Phys. Chem. A* **2002**, *106*, 2271.
20. Raschke, M. B.; Hayashi, M.; Lin, S. H.; Shen, Y. R. *Chem. Phys. Lett.* **2002**, *359*, 367.
21. Lin, S. H.; Hayashi, M.; Islampour, B.; Yu, J.; Yang, D. Y.; Wu, G. Y. C. *Physica B* **1996**, *222*, 191.
22. Liu, W.-K.; Hayashi, M.; Lin, J.-C.; Chang, H.-C.; Lin, S. H. *J. Chem. Phys.* **1997**, *106*, 5920.
23. Hayashi, M.; Shiu, Y.-J.; Liang, K. K.; Lin, S. H.; Shen, Y. R. *J. Phys. Chem. A* **2007**, *111*, 9062.
24. Heitler, W. *The Quantum Theory of Radiation*; Oxford University Press: London, 1953.
25. Shen, Y. R.; Ostroverkhov, V. *Chem. Rev.* **2006**, *106*, 1140.
26. Superfine, R.; Huang, J. Y.; Shen, Y. R. *Chem. Phys. Lett.* **1990**, *172*, 303.
27. Superfine, R.; Huang, J. Y.; Shen, Y. R. *Opt. Lett.* **1990**, *15*, 1276.
28. Ostroverkhov, V.; Waychunas, G. A.; Shen, Y. R. *Phys. Rev. Lett.* **2005**, *94*, 046102.
29. Tian, C.-S. et al. to be published, **2013**.
30. Lin, C.-K.; Shih, C.-C.; Niu, Y. L.; Tsai, M.-Y.; Shiu, Y.-J.; Zhu, C. Y.; Hayashi, M.; Lin, S. H. J. *Phys. Chem. C* **2013**, *117*, 1754.
31. Moad, J.; Simpson, G. J. *J. Phys. Chem. B* **2004**, *108*, 3548.
32. Wei, X.; Miranda, P. B.; Zhang, C.; Shen, Y. R. *Phys. Rev. B* **2002**, *66*, 085401.
33. Zhuang, X.; Miranda, P. B.; Kim, D.; Shen, Y. R. *Phys. Rev. B* **1999**, *59*, 12632.
34. Faraday, M. *Athenaeum* **1850**, *1181*, 640; *Philos. Mag.* **1859**, *17*, 162; *Proc. Roy. Soc. London* **1860**, *10*, 440.
35. Fletcher, N. H. *Philos. Mag.* **1968**, *18*, 1287.
36. Wei, X.; Miranda, P. B.; Zhang, C.; Shen, Y. R. *Phys. Rev. B* **2002**, *66*, 085401.

37. Du, Q.; Superfine, R.; Freysz, E.; Shen, Y. R. *Phys. Rev. Lett.* **1993**, *70*, 2313.
38. Baldelli, S.; Schnitzer, C.; Shultz, M. J.; Campbell, D. J. *J. Phys. Chem. B* **1997**, *101*, 10435.
39. Gan, W.; Wu, D.; Zhang, Z.; Feng, R. R.; Wang, H. F. *J. Chem. Phys.* **2006**, *124*, 114705.
40. Liu, D. F.; Ma, G.; Levering, L. M.; Allen, H. C. *J. Phys. Chem. B* **2004**, *108*, 2252.
41. Scatena, L. F.; Brown, M. G.; Richmond, G. L. *Science* **2001**, *292*, 908.
42. Wei, X.; Shen, Y. R. *Phys. Rev. Lett.* **2001**, *86*, 4799.
43. Sovago, M.; Campen, R. K.; Wurpel, G. W. H.; Muller, M.; Bakker, H. J.; Bonn, M. *Phys. Rev. Lett.* **2008**, *100*, 173901.
44. Nihonyanagi, S.; Ishiyama, T.; Lee, T.-K.; Yamaguchi, S.; Bonn, M.; Morita, A.; Tahara, T. *J. Am. Chem. Soc.* **2011**, *133*, 16875.
45. Du, Q.; Freysz, E.; Shen, Y. R. *Science* **1994**, *264*, 826.
46. Ji, N.; Ostroverkhov, V.; Tian, C. S.; Shen, Y. R. *Phys. Rev. Lett*. **2008**, *100*, 096102.
47. Tian, C.-S.; Shen, Y. R. *J. Am. Chem. Soc*. **2009**, *131*, 2790.
48. Shultz, M. J.; Baldelli, S.; Schnitzer, C.; Simonelli, D. *J. Phys. Chem. B* **2002**, *106*, 5313.
49. Raymond, E. A.; Tarbuck, T. L.; Richmond, G. L. *J. Phys. Chem. B* **2002**, *106*, 2817.
50. Raymond, E. A.; Tarbuck, T. L.; Brown, M. G.; Richmond, G. L. *J. Phys. Chem. B* **2003**, *107*, 546.
51. Allen, H. C.; Raymond, E. A.; Richmond, G. L. *J. Phys. Chem. A* **2001**, *105*, 1649.
52. Brown, M. G.; Raymond, E. A.; Allen, H. C.; Scatena, L. F.; Richmond, G. L. *J. Phys. Chem. A* **2000**, *104*, 10220.
53. Gan, W.; Wu, D.; Zhang, Z.; Guo, Y.; Wang, H. F. *Chin. J. Chem. Phys.* **2006**, *19*, 20.
54. Levering, L. M.; Sierra-Hernandez, M. R.; Allen, H. C. *J. Phys. Chem. C* **2007**, *111*, 8814.
55. Morita, A.; Ishiyama, T. *Phys. Chem. Chem. Phys*. **2008**, *10*, 5801.
56. Morita, A.; Hynes, J. T. *Chem. Phys.* **2000**, *258*, 371.
57. Ji, N.; Ostroverkhov, V.; Chen, C. Y.; Shen, Y. R. *J. Am. Chem. Soc.* **2007**, *129*. 10056.
58. Tian, C. S.; Ji, N.; Waychunas, G. A.; Shen, Y. R. *J. Am. Chem. Soc.* **2008**, *130*, 13033.
59. Tian, C. S.; Shen, Y. R. *Phys. Rev. Lett.* **2008**, *101*, 139401.
60. Pieniazek, P. A.; Tainter, C. J.; Skinner, J. L. *J. Am. Chem. Soc.* **2011**, *133*, 10360.
61. Sulpizi, M.; Salanne, M.; Sprik, M.; Gaigeot, M.-P. *J. Phys. Chem. Lett.* **2013**, *4*, 83.
62. Hayashi, M. et al., to be published, **2013**.
63. Wang, C.; Groenzin, H.; Shultz, M. J. *J. Phys. Chem. B* **2004**, *108*, 265.
64. Wang, C.; Groenzin, H.; Shultz, M. J. *J. Am. Chem. Soc.* **2005**, *127*, 9736.
65. Uosaki, K.; Yano, T.; Nihonyanagi, S. *J. Phys. Chem. B* **2004**, *108*, 19086.
66. Aliaga, C.; Baldelli, S.; Sum, A. *J. Phys. Chem. C* **2008**, *112*, 3064.
67. Miyamae, T.; Nozoye, H. *J. Photochem. Photobiol.* **2001**, *145*, 93.
68. Kataoka, S.; Gurau, M. C.; Albertorio, F.; Holden, M.; Lim, S.-M.; Yang, R.; Cremer, P. *Langmuir* **2004**, *20*, 1662.
69. Ye, S.; Kathiravan, A.; Hayashi, H.; Tong, Y.; Infahsaeng, Y.; Chabera, P.; Pascher, T.; Yartsev, A. P.; Isoda, S.; Imahori, H.; and Sundström, V. *J. Phys. Chem. C* **2013**, *117*, 6066.
70. Vogel, V. *Curr. Opin. Colloid Interface Sci*. **1996**, *1*, 257.
71. Castellana, E. T.; Cremer, P. S. *Surf. Sci. Rep.* **2006**, *61*, 429.
72. Lambert, A. G.; Davies, P. B.; Neivandt, D. J. *Appl. Spectrosc. Rev.* **2005**, *40*, 103.
73. Gopalakrishnan, S.; Liu, D. F.; Allen, H. C.; Kuo, M.; Shultz, M. J. *Chem. Rev.* **2006**, *106*, 1155.
74. Wang, H. F.; Gan, W.; Lu, R.; Rao, Y.; Wu, B. H. *Int. Rev. Phys. Chem.* **2005**, *24*, 191.
75. Ye, S. J.; Nguyen, K. T.; Le Clair, S.; Chen, Z. *J. Struct. Biol.* **2009**, *168*, 61.
76. Chen, X.; Wang, J.; Boughton, A. P.; Kristalyn, C. B.; Chen, Z. *J. Am. Chem. Soc.* **2007**, *129,* 1420.
77. Nguyen, K. T.; Le Clair, S.; Ye, S. J.; Chen, Z. *J. Phys. Chem. B* **2009**, *113*, 12169.
78. Ye, S. J.; Nguyen, K. T.; Chen, Z. *J. Phys. Chem. B* **2010**, *114*, 3334.
79. Chen, X.; Boughton, A. P.; Tesmer, J. J. G.; Chen, Z. *J. Am. Chem. Soc.* **2007**, *129*, 12658.
80. Ye, S. J.; Li, H. C.; Wei, F.; Jasensky, J.; Boughton, A. P.; Yang, P.; Chen, Z. *J. Am. Chem. Soc.* **2012**, *134*, 6237.
81. Fu, L.; Ma, G.; Yan, E. C. Y. *J. Am. Chem. Soc.* **2010**, *132*, 5405.
82. Fu, L.; Liu, J.; Yan, E. C. Y. *J. Am. Chem. Soc.* **2011**, *133*, 8094.
83. Perry, J. M.; Moad, A. J.; Begue, N. J.; Wampler, R. D.; Simpson, G. J. *J. Phys. Chem. B* **2005**, *109*, 20009.
84. Liu, C.; Monson, C. F.; Yang, T.; Pace, H.; Cremer, P. S. *Anal. Chem.* **2011**, *83*, 7876.
85. Clarke, M. L.; Wang, J.; Chen, Z. *J. Phys. Chem. B* **2005**, *109*, 22027.
86. Phillips, D. C.; York, R. L.; Mermut, O.; McCrea, K. R.; Ward, R. S.; Somorjai, G. A. *J. Phys. Chem. C* **2007**, *111*, 255.
87. York, R. L.; Mermut, O.; Phillips, D. C.; McCrea, K. R.;

Ward, R. S.; Somorjai, G. A. *J. Phys. Chem. C* **2007**, *111*, 8866.
88. Jung, S.-Y.; Lim, S.-M.; Albertorio, F.; Kim, G.; Gurau, M. C.; Yang, R. D.; Holden, M. A.; Cremer, P. S. *J. Am. Chem. Soc.* **2003**, *125*, 12782.
89. Mermut, O.; Phillips, D. C.; York, R. L.; McCrea, K. R.; Ward, R. S.; Somorjai, G. A. *J. Am. Chem. Soc.* **2006**, *128*, 3598.
90. Weidner, T.; Breen, N. F.; Drobny, G. P.; Castner, D. G. *J. Phy. Chem. B* **2009**, *113*, 15423.
91. Li, H.; Ye, S.; Wei, F.; Ma, S.; Luo, Y. *Langmuir* **2012**, *28*, 16979.
92. Wang, J.; Mark, A.; Chen, X.; Schmaier, A. H.; Waite, J. H.; and Chen, Z. *J. Am. Chem. Soc.* **2003**, *125*, 9914.
93. Yang, P.; Ramamoorthy, A.; Chen, Z. *Langmuir* **2011**, *27*, 7760.
94. Ding, B.; Chen, Z. *J. Phys. Chem. B* **2012**, *116*, 2545.
95. Wang, J.; Buck, S. M.; Mark, A.; Chen, Z. *J. Am. Chem. Soc.* **2002**, *124*, 13302.
96. Wang, J.; Buck, S. M.; Chen, Z. *J. Phys. Chem. B* **2002**, *106*, 11666.
97. Wang, J.; Paszti, Z.; Mark, A.; Chen, Z. *J. Phys. Chem. B* **2004**, *108*, 3625.
98. Wang, J.; Buck, S. M.; Chen, Z. *Analyst* **2003**, *128*, 773.
99. Wang, J.; Clarke, M. L.; Zhang, Y.; Chen, X.; Chen, Z. *Langmuir* **2003**, *19*, 7862.
100. Wang, J.; Clarke, M. L.; Chen, Z. *Anal. Chem.* **2004**, *76*, 2159.
101. York, R. L.; Holinga, G. J.; Somorjai, G. A. *Langmuir* **2009**, *25*, 9369.
102. Chen, X.; Tang, H.; Mark, A.; Wang, J.; Tew, G. N.; Chen, Z. *J. Am. Chem. Soc.* **2006**, *128*, 2711.
103. Nguyen, K. T.; Le Clair, S. V.; Ye, S.; Chen, Z. *J. Phys. Chem. B* **2009**, *113*, 12358.
104. Chen, X.; Wang, J.; Sniadecki, J. J.; Mark, A.; Chen, Z. *Langmuir* **2005**, *21*, 2662.
105. Nguyen, K. T.; King, J. T.; Chen, Z. *J. Phys. Chem. B* **2010**, *114*, 8291.
106. Xiao, D.; Fu, L.; Liu, J.; Batista, V. S.; Yan, E. C. Y. *J. Mol. Biol.* **2011**, *421*, 537.
107. Wurpel, G. W. H.; Sovago, M.; Bonn, M. *J. Am. Chem. Soc.* **2007**, *129*, 8420.
108. Campen, R. K.; Ngo, T. T. M.; Sovago, M.; Ruysschaert, J. M.; Bonn, M. *J. Am. Chem. Soc.* **2010**, *132*, 8037.
109. Asanuma, H.; Noguchi, H.; Uosaki, K.; Yu, H. Z. *J. Am. Chem. Soc.* **2008**, *130*, 8016.
110. Howell, C.; Schmidt, R.; Kurz, V.; Koelsch, P. *Biointerphases* **2008**, *3*, FC47.
111. Stokes, G. Y.; Gibbs-Davis, J. M.; Boman, F. C.; Stepp, B. R.; Condie, A. G.; Nguyen, S. B. T.; Geiger, F. M. *J. Am. Chem. Soc.* **2007**, *129*, 7492.
112. Walter, S. R.; Geiger, F. M. *J. Phys. Chem. Lett.* **2009**, *1*, 9.
113. Sartenaer, Y.; Tourillon, G.; Dreesen, L.; Lis, D.; Mani, A. A.; Thiry, P. A.; Peremans, A. *Biosens. Bioelectron.* **2007**, *22*, 2179.
114. Baugh, L.; Weidner, T.; Baio, J.; Nguyen, P. C. T.; Gamble, L. J.; Stayton, P. S.; Castner, D. G. *Langmuir* **2010**, *26*, 16434.
115. Ye, S.; Nguyen, K. T.; Boughton, A. P.; Mello, C. M.; Chen, Z. *Langmuir* **2009**, *26*, 6471.
116. Han, X.; Soblosky, L.; Slutsky, M.; Mello, C. M.; Chen, Z. *Langmuir* **2011**, *27*, 7042.
117. Wang, J.; Chen, X.; Clarke, M. L.; Chen, Z. *J. Phys. Chem. B* **2006**, *110*, 5017.
118. Liu, J.; Conboy, J. C. *J. Am. Chem. Soc.* **2004**, *126*, 8376.
119. Liu, J.; Conboy, J. C. *Biophys. J.* **2005**, *89*, 2522.
120. Anglin, T. C.; Liu, J.; Conboy, J. C. *Biophys. J.* **2007**, *92*, L01.
121. Anglin, T. C.; Brown, K. L.; Conboy, J. C. *J. Struct. Biol.* **2009**, *168*, 37.
122. Anglin, T. C.; Conboy, J. C. *Biophys. J.* **2008**, *95*, 186.
123. Liu, J.; Brown, K. L.; Conboy, J. *Faraday Discuss.* **2013**, *161*, 45.
124. Chen, X.; Wang, J.; Kristalyn, C. B.; Chen, Z. *Biophys. J.* **2007**, *93*, 866.
125. Chen, X.; Chen, Z. *Biochim. Biophys. Acta Biomembr.* **2006**, *1758*, 1257.

